NUMERICAL SIMULATIONS OF THERMAL-MIXING IN T-JUNCTION PIPING SYSTEM USING LARGE EDDY SIMULATION APPROACH

Masaaki TANAKA and Hiroyuki OHSHIMA

Thermal-hydraulic Research Group
Advanced Nuclear System Research and Development Directorate
Japan Atomic Energy Agency

Abstract

A numerical simulation code MUGTHES has been developed by the authors to investigate thermal striping phenomena related to high-cycle thermal fatigue in structure. The MUGTHES employs the large eddy simulation (LES) approach to predict unsteady thermal mixing phenomena and the boundary fitted coordinate system to fit complex boundary shapes in a reactor. In this paper, a part of the verification and validation (V&V) study of the MUGTHES is introduced and numerical simulations of a T-junction piping system (T-pipe) are described. The V&V examinations are conducted with fundamental problems in literatures with a concept of the phenomena identification ranking table (PIRT). After the V&V examinations, thermal striping phenomena in a T-pipe are numerically investigated by the MUGTHES with the LES approach. As for the boundary conditions, two typical flow patterns of a wall jet and an impinging jet conditions are chosen from the WATLON experiment which is a water experiment at the JAEA using a T-pipe. The numerical results are validated by comparing with measured velocity and temperature profiles. Characteristic large-scale vortex structures are identified around the branch pipe jet in the mixing process. The generation mechanism of temperature fluctuation in the T-pipe is revealed in relation with the large-scale vortex structures.

1. INTRODUCTION

Conceptual design study of an advanced sodium-cooled fast reactor the Japan Sodium cooled Fast Reactor (JSFR) has been conducted at the Japan Atomic Energy Agency (JAEA) (Ichimiya, 2007). Figure 1 outlines a thermal striping issue in the upper plenum of the JSFR reactor vessel (Tanaka et al., 2009a). There is the Upper Internal Structure (UIS) in the plenum and the lowest perforated plate of the UIS is the Core Instruments Plate (CIP) which holds upper guide tubes and driving shafts of control rod systems, thermocouples and the other sensors for operating and safety measures (Ohyama et al., 2009). Below the CIP, hot sodium comes from fuel subassemblies and cold sodium flows out from control rod channels at the top of the reactor core. When temperature fluctuation caused by turbulence mixing of the coolants at different temperatures is transmitted to the CIP surface, cyclic thermal stress may be induced in the structure according to the frequency characteristics and the degree of amplitude of the fluid temperature fluctuation on the structure surface. Since the continuous cyclic stress on the structure may cause crack initiation and crack growth, thermal mixing phenomena called as thermal striping has been recognized as one of the most important issues in design and safety of the JSFR (Ohyama et al., 2009, Tanaka et al., 2009a and Kobayashi et al., 2009). A numerical simulation code MUGTHES has been developed by

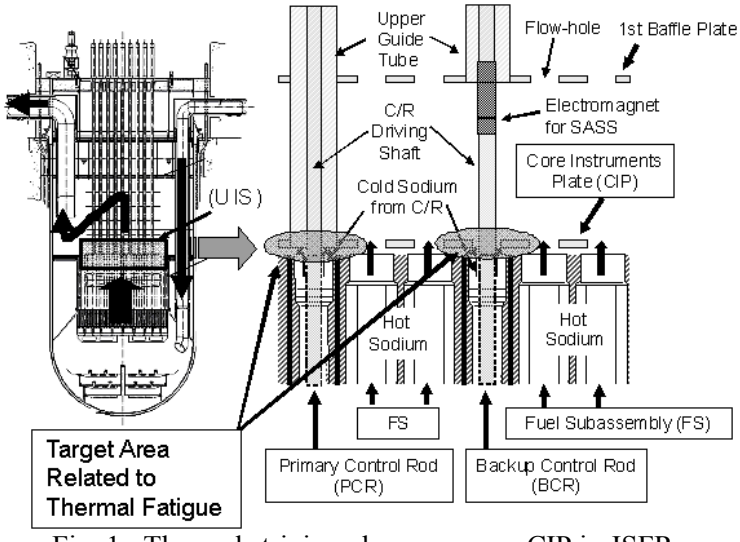

Fig. 1: Thermal striping phenomena on CIP in JSFR.

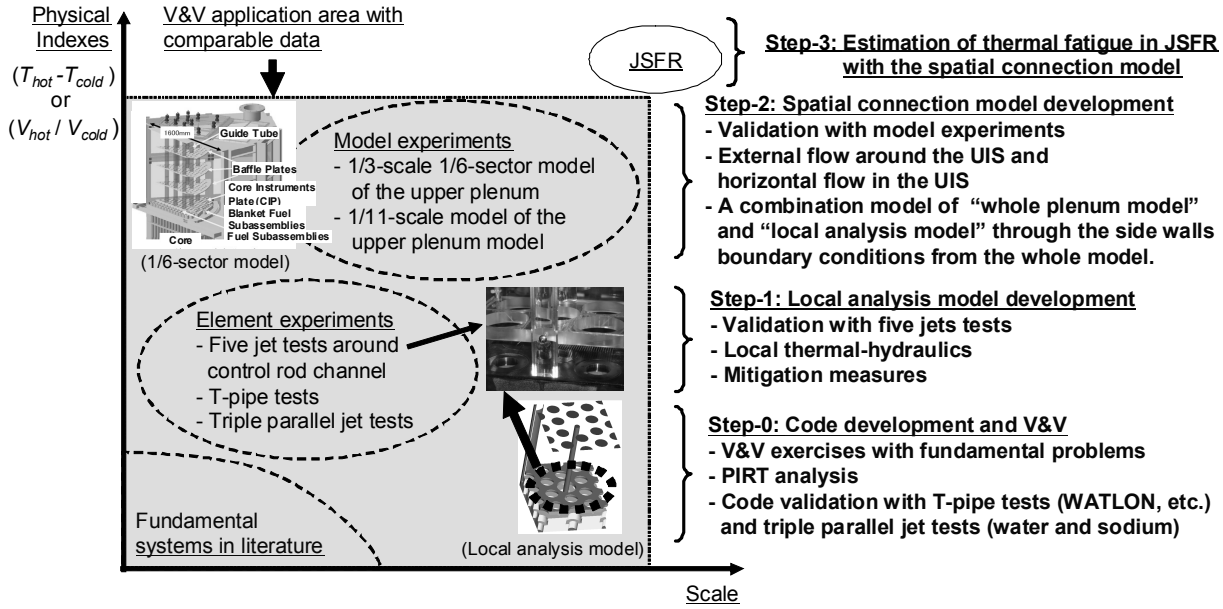

Fig. 2: Numerical estimation method development for the thermal fatigue on the CIP in the JSFR and relation between the JSFR condition and the V&V application area with comparable data.

the authors at the JAEA (Tanaka et al., 2009b) in addition to the experimental investigations (Kimura et al., 2010). From viewpoint of recent progress in computer capacity, numerical simulation can be an efficient tool to investigate the thermal fatigue in structure and to provide the useful information (e.g. spatial distribution and frequency characteristics of temperature) for the high-cycle thermal fatigue estimation method of the JSFR. Moreover, direct estimation of the high-cycle thermal fatigue by the numerical simulation is desired in the JSFR design study because it is difficult for model experiments to cover the JSFR operation conditions. Figure 2 shows a strategy of numerical estimation method development for the thermal fatigue on the CIP in the JSFR (Tanaka et al., 2009a) and relation between the JSFR condition and the V&V application area with comparable data. At Step-0, numerical simulation code development and its verification and validation (V&V) study is to be conducted in fundamental systems and typical element experiments with comparable data in literatures. At Step-1, numerical estimation method in a limited area around a target control rod channel is to be developed to investigate the local thermal-hydraulics and to consider mitigation measures against the significant temperature fluctuation. At Step-2, the method which can consider external circumferential flow around the UIS is to be developed because the cold sodium jets from blanket fuel subassemblies are certainly affected by the external flow and also the influence of horizontal flow in the UIS should be considered. At the final Step-3, thermal fatigue on the CIP in the JSFR is to be estimated by the code and the method which are sufficiently developed and validated at steps from Step-0 to Step-2.

In this paper, the V&V process for the step-by-step development approach as shown in Fig. 2 is introduced and numerical simulations for a T-junction piping system (T-pipe) as a code validation are described. Before application of the MUGTHES to a T-pipe simulation, concept of the V&V process in the development steps and application of a concept of the phenomena identification ranking table (PIRT) analysis in validation problems selection are introduced. Focusing on activities at Step-0, numerical simulations for fundamental problems at laminar flow conditions as verification of numerical schemes and discretization methods in the MUGTHES and the numerical simulations for fundamental problems at turbulent flow condition as validation of the large eddy simulation (LES) approach assembled in the MUGTHES are briefly described. Thermal striping phenomena in a T-pipe are numerically investigated in order to confirm applicability of the LES approach in the MUGTHES and to investigate the characteristics of the thermal mixing phenomena relating to the large-scale vortex structure generation. Numerical results with several coefficients Cs=0.1, 0.14, 0.17 of the standard Smagorinsky model in the LES approach are validated by comparisons with the experimental results of velocity and temperature to find out an applicable model coefficient (Cs). Through the T-pipe simulations, generation mechanism of temperature fluctuation in the T-pipe is discussed in relation to the large-scale vortex structures.

2. OUTLINE OF NUMERICAL SIMUALTION CODE

A numerical simulation code MUGTHES employs the LES approach to predict unsteady thermal mixing phenomena and the boundary fitted coordinate (BFC) system to fit complex boundary shapes in a reactor (Tanaka et al., 2009b). The MUGTHES is designed to simulate the thermal interaction between unsteady thermal-hydraulics and unsteady heat conduction in structure simultaneously. In the thermal-hydraulics module which is only used in this study, unsteady incompressible Navier-Stokes equation and energy conservation equation are solved by using a finite volume approach and finite differential scheme. A collocated grid system is employed and then physical velocity components (u,v,w) in a Cartesian coordinate system, temperature T and pressure P are defined at the center of the computational cell. In the BFC system, additional terms of Jacobian J and surface area vectors called as "metrics" exist and they are evaluated based on the finite volume approach and on their physical meanings (Tanaka et al., 2009b). The turbulent viscosity μ_t is evaluated by the standard Smagorinsky model as follows.

$$\mu_t = \rho(Csf\Delta)^2\left|\overline{D}\right| \tag{1}$$

$$f = 1-\exp\left(-\delta^+/25\right) \tag{2}$$

$$\Delta = J^{1/3} \tag{3}$$

$$\left|\overline{D}\right| = \sqrt{2\overline{D_{ij}}\,\overline{D_{ij}}} \tag{4}$$

$$\overline{D_{ij}} = \frac{1}{2}\left(\frac{\partial \overline{u_i}}{\partial x_j}+\frac{\partial \overline{u_j}}{\partial x_i}\right) = \frac{1}{2J}\left(\frac{\partial}{\partial \xi_l}\left(J\frac{\partial \xi_l}{\partial x_j}\overline{u_i}\right)+\frac{\partial}{\partial \xi_m}\left(J\frac{\partial \xi_m}{\partial x_i}\overline{u_j}\right)\right) \tag{5}$$

Here, Cs is parameter coefficient of the model and Δ is the filter length evaluated with the Jacobian J corresponding to the cell volume. D_{ij} is rate of strain tensor defined at the cell center in the BFC system. In boundary cells on walls, van Driest damping function in Eq. (2) is used. Since our goal is to numerically estimate unsteady thermal-hydraulics and thermal fatigue in the large-scale system JSFR, artificial wall conditions (Morinishi and Kobayashi, 1989) derived by a wall function law (Temmerman et al., 2003) is considered in the LES approach in order to utilize a coarse mesh arrangement near wall region and to suppress computational load for a long time transient calculation in the large system (Tanaka et al., 2009b).

The Crank-Nicolson method is used for time integration and the Projection method (Chorin, 1968) is used to solve velocity field. The second order central differential scheme is used for the advection term in the momentum equation. As for the pressure solver, an iterative method BiCGSTAB+SOR (Tanaka et al., 2009b) is used. Velocity components are corrected by using the correct pressure distribution. The energy equation is solved using the velocity components at a new time step. The monotone integrated large eddy simulation (MILES) approach (Gullbrand and Chow, 2003) which has been successfully used in numerical simulations of thermal striping phenomena (Tanaka et al., 2009a, Kamide et al., 2009 and kimura et al., 2001) is used in this study. In the MILES approach, numerical diffusion (error) derived from a higher order upwind scheme is taken as an implicit model of turbulence diffusion. Then, a higher order accuracy upwind scheme (Kajishima, 1997) in the BFC system is used for the advection term in the energy equation without the explicit thermal diffusion model. A simple limiting procedure is employed to prevent over- and under-estimation of the temperature distribution around the steep temperature gradient (Tanaka et al., 2009b).

3. VERIFICATION AND VALIDATION STUDY

3.1 V&V Process with PIRT Analysis

We have considered V&V process referring to several literatures for the V&V of computational fluid dynamics (CFD) (ANS, 1998, Oberkampf and Trucano, 2002, AIAA, 2002, and ASME, 2009). Scale of the JSFR as our goal is too large to conduct parametric studies required for the V&V and it is difficult to obtain comparable data of the JSFR by experiments. Then, we tried to arrange the V&V process for the step-by-step development strategy as shown in Fig. 2. The important idea is to prepare a potentially applicable numerical simulation code with necessary models and method for thermal fatigue estimation in the JSFR at the end of the V&V process. We stated that the verification is performed through

Table 1: PIRT analysis of the T-pipe thermal mixing for validation problems identification.

Phenomena transitions	Element phenomena and factors	Relating problems
(1)Branch pipe jet into the main pipe	Branch pipe jet in main pipe	Free jets into the plenum or Jet in cross flow
	Shear layer instability	Shear layer flow
		Viscosity driven cavity flow
	Flow through branch pipe jet	Flow around obstacle
(2) Thermal mixing	Cyclic flow fluctuation/ Vortex generation	Flow through circular cylinder
		Back-facing step flow
	Wake formation	
	Secondary flow in branch pipe jet	Pipe elbow flow with short curvature radius
		Flow in square duct
	Buoyancy effect in the wake	Buoyancy driven cavity flow
(3) Pipe flow in upstream and downstream	Surface roughness, piping layout and Reynolds number	Pipe flow
		Pipe elbow flow

numerical simulations for fundamental problems at laminar flow conditions to confirm accuracy of the numerical schemes and methods except the LES approach, and the validation is performed through the numerical simulations at a turbulence flow condition to confirm applicability of the code to practical problems. In this study, two aspects of validation are considered: one is the validation of the physical models (the LES approach) in the code and another is the validation of the code and the method as a complete system. According to the idea that right results in the validation imply that the model is solved correctly (AIAA, 1998), fundamental problems and relatively small-scale element experiments at turbulence conditions are positioned at Step-0 and Step-1 as shown in Fig.2 in viewpoint of the model validation. Large-scale model experiments for the JSFR are shown at Step-2 for the validation of the code and the method as a complete system. A concept of the PIRT (Oberkampf and Trucano, 2002) is utilized in order to specify the problems in the validation process on the subject to a target system and phenomena.

3.2 Implementation of Verification and Validation of the MUGTHES

V&V examinations of the MUGTHES were performed in accordance with the proposed process in Sec.3.1 before the application to the T-pipe simulation. Verification examinations were performed through the numerical simulations at laminar flow conditions in fundamental systems; (1) viscosity driven square cavity (Ghia et al., 1982), (2) Backward-facing step flow (Denham and Patrick, 1974), (3) Pipe elbow flow in large curvature radius (Bovendeerd et al., 1987) and (4) Buoyancy force driven square cavity flow (Davis, 1983). Table 1 listed the phenomena transitions of thermal mixing in a T-pipe along the flow direction: (1) branch pipe jet entering into the main pipe, (2) thermal mixing and (3) pipe flow in upstream and downstream. Fundamental problems relating to the element phenomena and factors were extracted as candidates for the validation examinations. Problems of (1) square duct flow (Sata et al., 1994), (2) flow around surface-mounted obstacle (Martinuzzi and Tropea, 1993), (3) backward-facing step flow (Kasagi and Matsunaga, 1995) and (4) flow through circular cylinder (Pradera et al., 2007) were selected for the validation of the MUGTHES in viewpoint of the LES approach. By comparing the numerical results of the MUGTHES with the experimental and computational results in literatures, adequacy of the numerical schemes and models in the MUGTHES could be confirmed and it could be confirmed that the MUGTHES had potential to solve the flow field in the T-pipe problem (Tanaka, 2010).

4. NUMERICAL SIMULATIONS FOR WATLON EXPERIMENT

4.1 Flow Patterns of Branch Pipe Jet in Main Pipe.

A T-junction piping system (T-pipe) for mixing fluids at different temperatures is especially important part in viewpoint of the thermal striping generation causing thermal fatigue in structure. In fact, events

relating to the thermal fatigue were happen at T-pipes in nuclear power plants (Nordgren, 1983, Chapuliot, 2005 and IAEA, 2002). In Japan, guideline for high-cycle thermal fatigue estimation of a pipe in a light water reactor (JSME, 2003) was published. As for the JSFR, an estimation method for the thermal fatigue has been investigated (Kasahara et al., 2005 and Kimura et al., 2010). The WATLON experiment has been conducted at JAEA to provide comparable data for the code validation and for the estimation method establishment (Igarashi et al., 2003). The test section consists of a horizontal main pipe of 0.15 m in diameter and a vertical branch pipe of 0.05 m in diameter. From the flow visualization test, it was indicated that that flow patterns of the branch pipe jet in the main pipe flow could be classified into three categories: (1) impinging jet, (2) deflecting jet and (3) wall jet according to the valance of the inertia forces between the main pipe flow and the branch pipe jet as follow.

$$M_R = M_m / M_b = \left[\rho_m W_m^{\,2} \cdot (D_m \cdot D_b)\right] / \left[\rho_b V_b^{\,2} \cdot \left(\pi D_b^{\,2}/4\right)\right] \quad (6)$$

$$\text{if} \quad M_R > 1.35 \qquad \text{(Wall jet)} \quad (7a)$$

$$\text{if} \quad 1.35 > M_R > 0.35 \qquad \text{(Deflecting jet)} \quad (7b)$$

$$\text{if} \quad 0.35 > M_R \qquad \text{(Impinging jet)} \quad (7c)$$

Here, ρ is a fluid density and D is a pipe diameter. D_m(=150 mm) is for a straight horizontal main pipe and D_b (=50 mm) is for a vertical branch pipe. Subscripts of $_m$ and $_b$ mean main pipe and branch pipe, respectively. W_m and V_b are bulk velocities at the inlet boundaries of the horizontal main pipe and the vertical branch pipe, respectively. In the investigation of jet in cross-flow relating to the branch pipe jet in the T-pipe, the slope of the jet axis depends on the ratio between the inertia of cross flow $\rho_m(W_m)^2$ and that of branch jet $\rho_b(V_b)^2$ (Muppidi and Mahesh, 2007 and Marzouk and Ghoniem, 2007). This supports the categorization idea in Eq. (6) and (7). Figures 3(a) and (b) show instantaneous pictures of the branch pipe jet in the main pipe at (a) an impinging jet case and (b) a wall jet case in the WATLON experiment. Figures 4(a) and (b) show instantaneous color images of a liquid crystal sheet attached on the main pipe surface at (a) an impinging jet case and (b) a wall jet case in the WATLON experiment (Tanaka, 2006). At both cases in Fig. 4(a) and (b), cold fluid seen as brown color touches and forms a wide spot on the main pipe surface and significant temperature fluctuation on the main pipe surface may be caused around the spot.

4.2 Numerical conditions

Table 2 lists boundary conditions at two typical flow patterns of an impinging jet and a wall jet in the T-pipe WATLON experiment (Igarashi et al., 2003) employed for the validation of the MUGTHES in thermal problems (see Fig. 2). Figure 5 shows the BFC mesh arrangement for the numerical simulation of the WATLON experiment. Total number of the cells in the mesh arrangement was 262,480. The origin of the coordinate axes was positioned at the point where the center axis of the branch pipe connects with the main pipe. The origin was called the "connecting point". In the simulation, distance to the inlet boundary surface from the connecting point was $2D_m$ and that to the outlet boundary from the connecting point was $4D_m$. The main pipe flow went from the right to the left, and the branch pipe jet came from below. Gravity direction was along the negative direction of y from the main pipe to the branch pipe inlet in the same manner as the experiment. The numerical simulation at the case of WJ2 with Cs=0.14 in the same mesh arrangement as shown in Fig. 5 was previously conducted by the authors (Tanaka, 2009b). Duration time of transient calculation was extended to 10 s in the present simulation from 8 s in the previous simulation. At the inlet boundaries of the main pipe and the branch pipe, fixed velocity profile without the velocity fluctuation was applied as the Table 2. In the impinging jet cases, flat velocity profile was applied at the main pipe inlet. In the wall jet cases,

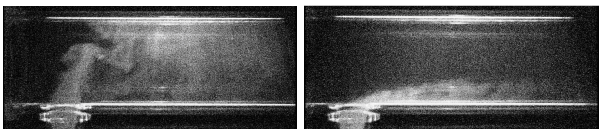

(a) Impinging jet (b) Wall jet

Fig. 3: Instantaneous pictures of branch pipe jet in a T-pipe (Branch pipe jet contains fluorescent dye).

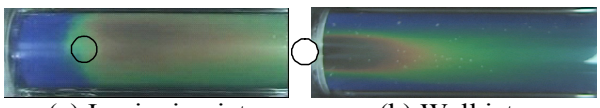

(a) Impinging jet (b) Wall jet

Fig. 4: Instantaneous picture of temperature distribution on main pipe surface taken by a color image of liquid crystal sheet.

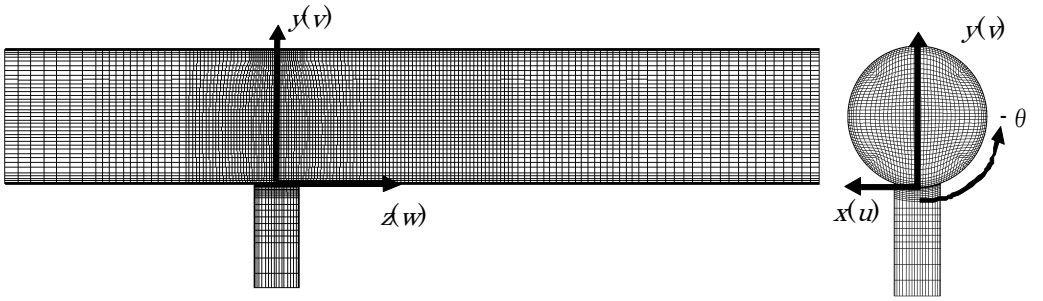

(a) Side View (b) Cross-Section (View from inlet)

Fig. 5: Mesh arrangement in numerical simulation for the WATLON experiment.

turbulent velocity profile by using the 1/7th power law was applied to the main pipe inlet and the branch pipe inlet. It was confirmed that the time averaged velocity profiles of numerical simulation were not far from those of the experimental data. As the next step of the code development, the authors are going to be checked influence of the velocity profiles at the inlet in addition to developing the velocity fluctuation generation method. As the inlet boundary conditions for the energy, constant temperature was applied to each pipe inlet. Adiabatic condition was set on the inner surface of the pipes and outlet of the main pipe. After a quasi-steady state calculation to achieve developed state, transient calculation was performed for approximately 10 s with the time interval of 0.1 ms. And 4,000 data points of velocity components and temperature were collected for statistical analysis with the time interval of 1 ms. Fluctuation intensity was evaluated by the standard deviation.

Table 2: Employed Boundary Conditions.

Case	*Cs*	Main Pipe			Branch Pipe		
		T_m (°C)	W_m (m/s)	Re	T_b (°C)	V_b (m/s)	Re
WJ1	0.10	48.0	1.46	3.8×10^5	33.0	1.0	6.6×10^4
WJ2	0.14						
WJ3	0.17						
IJ1	0.10		0.23	5×10^4			
IJ2	0.14						
IJ3	0.17						

4.3 Mixing Phenomena in the T-pipe

Figures 6(a) and (b) show the instantaneous fluid temperature distributions on the symmetric axial cross section at the impinging jet (IJ2) and the wall jet (WJ2) conditions respectively. In the figures, the branch pipe jet at low temperature of 33 °C (=T_b) seen as blue enters into the main pipe flow at high temperature of 48 °C (=T_m) in red area. Figures 7(a) and (b) show fluid temperature fluctuation intensity distributions on the symmetric axial cross section at the impinging jet (IJ2) and the wall jet (WJ2) conditions respectively. Figures 8(a) and (b) show the instantaneous large-scale vortex structures at the impinging jet (IJ2) and the wall jet (WJ2) conditions respectively. The vortex structures were described by using the iso-surface of the second invariant of velocity gradient defined by the following equation.

$$Q = \left(W_{ij}W_{ij} - D_{ij}D_{ij}\right)/2 \tag{8}$$

$$\overline{W_{ij}} = \frac{1}{2}\left(\frac{\partial \overline{u_i}}{\partial x_j} - \frac{\partial \overline{u_j}}{\partial x_i}\right) = \frac{1}{2J}\left(\frac{\partial}{\partial \xi_l}\left(J\frac{\partial \xi_l}{\partial x_j}\overline{u_i}\right) - \frac{\partial}{\partial \xi_m}\left(J\frac{\partial \xi_m}{\partial x_i}\overline{u_j}\right)\right) \tag{9}$$

Here, W_{ij} is rotation component and D_{ij} is shear strain tensor defined by Eq. (5). Threshold value of Q s^{-2} is decided through the observations of the iso-surface of vorticity, fluid temperature and velocity components. Q=600 s^{-2} is for the impinging jet case and Q=2,000 s^{-2} is for the wall jet case. The shape of the vortex structure drawn by the iso-surface of Q s^{-2} is much sharper than that by the vorticity. Figures 9(a) and (b) show turbulence energy intensity k distributions at the impinging jet (IJ2) and the wall jet (WJ2) conditions respectively.

At the impinging jet case with Cs=0.14 (IJ2) as shown in Fig. 6(a), Fig. 7(a), Fig. 8(a) and Fig. 9(a), the magnitude of momentum inertia of the branch pipe flow was superior to that of the main pipe flow and

then the branch pipe jet easily came into the center region of the main pipe with little bend. Wavy temperature boundaries appeared around the branch pipe jet as shown in Fig. 6(a) and also temperature fluctuation intensity was high around the jet as shown in Fig. 7(a). In front of the jet, the wavy boundary was much clearer and the fluctuation intensity was much higher than those behind the jet. The periodical large-scale vortex structures were shown in front of the branch pipe jet as shown in Fig. 8(a). In front of the jet, hot fluid of the main stream was caught between the large-scale vortex structures at low temperature. Then, the branch pipe jet conveyed the hot and cold striped temperature distribution to the upper part of the main pipe and the thermal striping could be caused on the upper surface. Thus, the high fluctuation intensity of fluid temperature in front of the jet (see Fig. 7(a)) was caused by the large-scale vortex motions (see Fig. 8(a)). Periodical vortex structures generation were indicated in the T-pipe simulation by Nakamura et al. (2009) and also in the JIC (jet in Cross flow) investigations at low Reynolds number conditions by Marzouk and Ghoniem (2007) and Fric and Roshko (1994). After impinging on the upper surface, cold fluid from the branch pipe jet flowed to downstream through near upper wall region. Behind the jet, three-dimensional flow behaviour consisting of the periodical flow like Karman vortex streak on the horizontal plane and the symmetrical circumferential flows on the transversal cross section was shown. The three-dimensional flow brought high temperature fluctuation intensity (Fig. 7(a)) and high turbulence energy intensity (Fig. 9(a)) around the lower boundary of the cold jet tail as shown in Fig. 6(a) in the upper part of the main pipe. On the lower half part of the main pipe, temperature fluctuation was not high behind the branch pipe jet though turbulence energy intensity was high as shown in Fig. 9(a). In this region, main stream going around the branch pipe jet was mainly fluctuated without the thermal mixing.

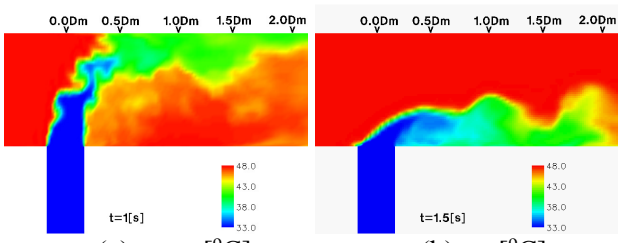

(a) [^{o}C] (b) [^{o}C]

Fig. 6: Instantaneous distributions of fluid temperature on symmetric axial cross section at (a) impinging jet (IJ2) and (b) wall jet (WJ2) cases.

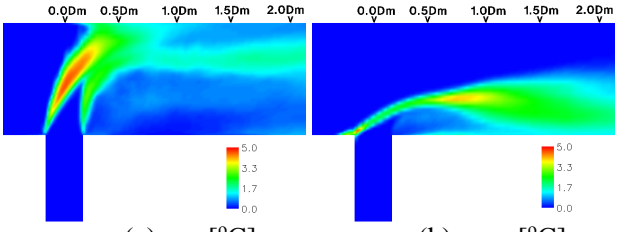

(a) [^{o}C] (b) [^{o}C]

Fig. 7: Fluid temperature fluctuation intensity distributions on symmetric axial cross section at (a) impinging jet (IJ2) and (b) wall jet (WJ2) cases.

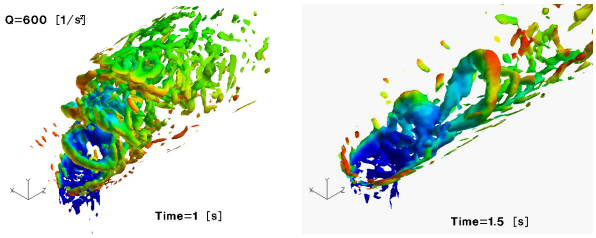

(a) (b)

Fig. 8: Instantaneous distributions of large-scale vortex structures at (a) impinging jet (IJ2) and (b) wall jet (WJ2) cases (Vortex structures are described by Q=600 1/s^2 at (a) and Q=2,000 s^{-2} at (b), and color shows fluid temperature as the same in Fig.6).

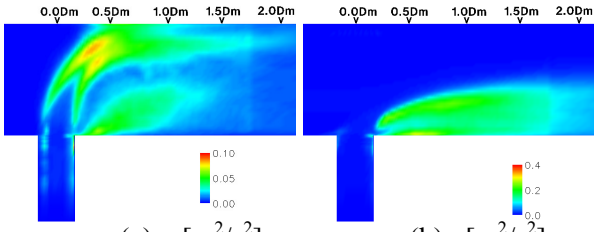

(a) [m^2/s^2] (b) [m^2/s^2]

Fig. 9: Turbulence energy intensity k distributions on symmetric axial cross section at (a) impinging jet (IJ2) and (b) wall jet (WJ2) cases.

At the wall jet case (WJ2) as shown in Fig. 6(b), Fig. 7(b), Fig. 8(b) and Fig. 9(b), the magnitude of momentum inertia of the main pipe flow was superior to that of the branch pipe flow. Then, the main pipe flow could bend the vertical branch pipe jet to the horizontal direction and the jet went through the lower half cross section forming a wake region as shown in Fig. 6(b). At the front edge of the branch pipe, temperature fluctuation intensity was high as shown in Fig. 7(b). Intermittent reverse flows along

the main pipe surface from the branch pipe end on the upstream side could cause high temperature fluctuation intensity. Attention of thermal fatigue occurrence should be paid at the front edge of the branch pipe in addition to the downstream region. High fluid temperature fluctuation intensity starting from the branch pipe end on upstream side as shown in Fig. 7(b) was caused by the up-and-down swing motion of the top surface of the branch pipe jet boundary due to the inertial valance between the main pipe flow and the branch pipe jet. After the jet enters into the main pipe, a wavy temperature boundary appeared in the center part of the main pipe above the wake. In Fig. 8(b), large-scale hairpin vortex structures existed behind the branch pipe jet not in front of it. Compared with the results in Fig. 6(b) and Fig. 8(b), the tops of the hairpin vortex structure corresponded to those of the wavy temperature boundaries. Due to the hairpin vortex structure motion, cold fluid was detached from the branch pipe jet end. And the vortex structure conveyed the cold fluid to the downstream. Additionally, it was recognized that the hairpin vortex structure provided cold fluid to the wake in accordance with its rotating motion (Tanaka, 2009b). As for such large-scale vortex structures, Hibara et al. (2004) successfully visualized the hairpin vortex structures generated in the T-pipe water experiment at laminar flow conditions and Sau and Mahesh (2007) predicted the hairpin vortex structure in the jet in cross flow at low Reynolds number condition (Re_b<600) by using the direct numerical simulation. Tanaka et al. (2004) indicated hairpin vortex structure existence in the T-pipe with elbow pipe in upstream side by the numerical simulation at high Reynolds number conditions of $Re_m=1.1\times10^5$ and $Re_b=2.1\times10^4$. Nakamura et al. (2009) did a detached eddy simulation (DES) for the WATLON experiment at the same boundary conditions listed in Table 2 and they indicated the contribution of the hairpin vortex structure to the temperature fluctuation in the T-pipe.

The large-scale vortex structures formed in front of the branch pipe jet at the impinging jet case and the large-scale hairpin vortex structures formed behind the branch pipe jet at the wall jet case had a very important role in the thermal striping phenomena in the T-pipe. And, temperature fluctuation distribution is not necessarily conjectured by the velocity fluctuation distribution directly and the large-scale vortex motion should be considered in order to predict the significant temperature fluctuation generation in viewpoint of the thermal fatigue on the pipe surface.

4.4 Comparisons between Experimental and Numerical Results in Impinging Jet Case

Figures 10 (a) and (b) respectively show vertical profiles of (a) the time-averaged axial velocity and (b) the axial velocity fluctuation intensity on the symmetric axial cross-section at (1) $0.5D_m$ and (2) $1.0D_m$ downstream from the connecting point at the impinging jet cases IJ1(Cs=0.1), IJ2(Cs=0.14) and IJ3(Cs=0.17). The time-averaged axial velocity W and the fluctuation intensity W' were normalized by the mean axial velocity at the inlet W_m as in Table 2. The time-averaged velocity profiles of IJ2 (Cs=0.14) as in Figs. 10(a-1) and (a-2) almost agreed with those of the experimental results. However, the under-estimation of the axial velocity was shown from y/D_m=0.2 to y/D_m=0.6 as shown in Fig. 10(a-1). The flow in the wake behind the branch pipe jet was similar to that behind the rigid cylinder for the Karman's vortex streak and the axial velocity magnitude was almost stagnant. It could be considered that the difference between the experimental results and the numerical results was due to the limitation of the standard Smagorinsky model. Then, the LES model is going to be modified to fit the stagnant flow in the wake region. The high axial velocity was shown at around y/D_m=0.8 because the branch pipe jet impinging to the upper

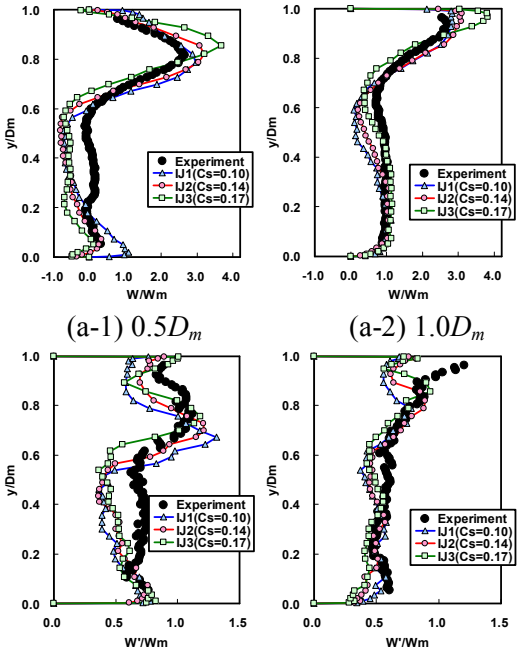

(a-1) $0.5D_m$ (a-2) $1.0D_m$

(b-1) $0.5D_m$ (b-2) $1.0D_m$

Fig. 10: Vertical profiles of (a) time average and (b) fluctuation intensity of axial velocity component through the main pipe center axis at two typical positions in the impinging jet case.

surface went through this region to the downstream. The axial velocity fluctuation was also high at around y/D_m=0.8 due to the three-dimensional flow behavior (as shown in Fig. 9(a)).

Figures 11 (a) and (b) respectively show vertical profiles of (a) the time-averaged fluid temperature and (b) the fluid temperature fluctuation intensity on the symmetric axial cross section at (1) $0.5D_m$ and (2) $1.0D_m$ downstream from the connecting point at the impinging jet cases IJ1 (Cs=0.10), IJ2 (Cs=0.14) and IJ3 (Cs=0.17). The time-averaged temperature difference (T-T_b) in Fig. 11(a) and the fluctuation intensity T' in Fig. 11(b) were normalized by the fluid temperature difference before mixing $dT=T_m-T_b$. As for the time-averaged temperature profiles in Fig. 11(a-1) and (a-2), numerical results of IJ2 (Cs=0.14) showed good agreement with the experimental results. However, the other cases of Cs=0.1 and 0.17 did not succeed to predict the experimental results. The temperature fluctuation intensity of the numerical results in all cases was almost half level of that of the experimental results in upper part of the main pipe (y/D_m>0.6).

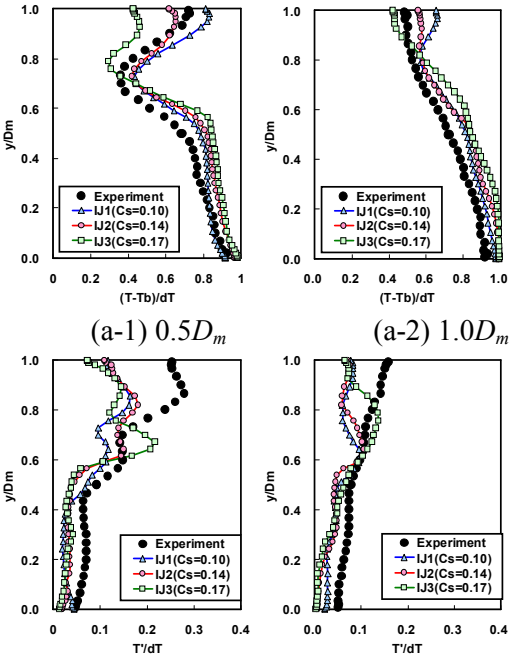

(a-1) $0.5D_m$ (a-2) $1.0D_m$

(b-1) $0.5D_m$ (b-2) $1.0D_m$

Fig.11: Vertical profiles of (a) time average and (b) fluctuation intensity of fluid temperature through the main pipe center axis at two typical positions in the impinging jet case.

At this moment, it can be recognized that the numerical results with Cs=0.14 are more acceptable than other results with Cs=0.1 and 0.17, though the difference between the experimental and numerical results in temperature fluctuation still remains.

4.5 Comparisons between Experimental and Numerical Results in Wall Jet Case

Figures 12 (a) and (b) respectively show vertical profiles of the time-averaged axial velocity and the axial velocity fluctuation intensity on the symmetric axial cross-section at (1) $0.5D_m$ and (2) $1.0D_m$ downstream from the connecting point. The time-averaged axial velocity W and the fluctuation intensity W' were normalized by the mean axial velocity at the inlet W_m as in Table 2. The time-averaged velocity profiles in Figs.12 (a-1) and (a-2) showed good agreement between the experimental and numerical results in all Cs cases though influence of the velocity profile evaluated by the power law at the inlet slightly existed at around y/D_m=0.6. The main stream accelerated as decreasing effective pipe area by the wake formation due to the branch pipe jet entering into the main pipe (axial velocity was approximately 1.2 times higher than that before the mixing). The reverse flow (y/D_m<0.5) in the wake was not shown at $1.0D_m$ downstream from the connecting point. As for the axial velocity fluctuation as shown in Figs.12 (b-1) and (b-2), numerical results could almost trace the trend of experimental results. Under estimation of the fluctuation intensity at all cases in the upper part of the main pipe (y/D_m>0.5) was due to the

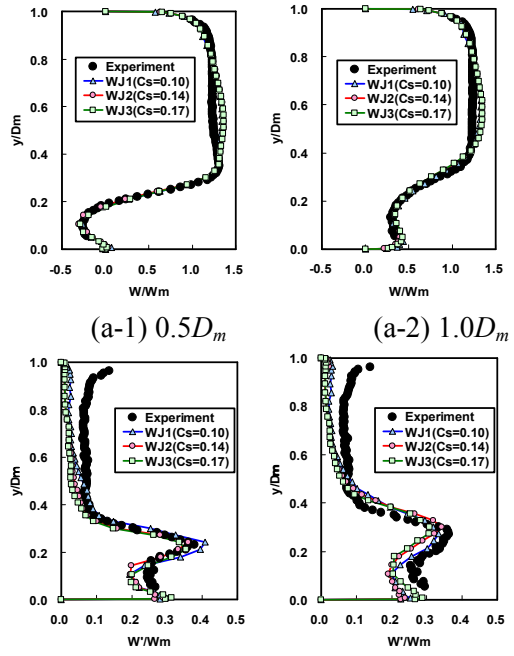

(a-1) $0.5D_m$ (a-2) $1.0D_m$

(b-1) $0.5D_m$ (b-2) $1.0D_m$

Fig. 12: Vertical profiles of (a) time average and (b) fluctuation intensity of axial velocity component through the main pipe center axis at two typical positions in the wall jet case.

constant velocity profile at the inlet. Axial velocity fluctuation at the inlet was not considerd in this study and effect of the velocity fluctuation feed at the inlet is gong to be checked as the next step of the code development. The highest fluctuation intensity at approximately y/D_m=0.2 was not owing to the tubulence fluctuation by small-scale eddies in the stream, but owing to the hairpin-shaped large-scale vortices as shown in Fig. 8(b). The fluctuation intensity profiles of numerical simulation with Cs=0.14 (WJ2) on the branch pipe side (y/D_m<0.5) almost agreed with those of the experiment and the fluctuation intensity at the case of WJ1(Cs=0.10) was higher than that at the case of WJ2(Cs=0.14) and WJ3(Cs=0.17).

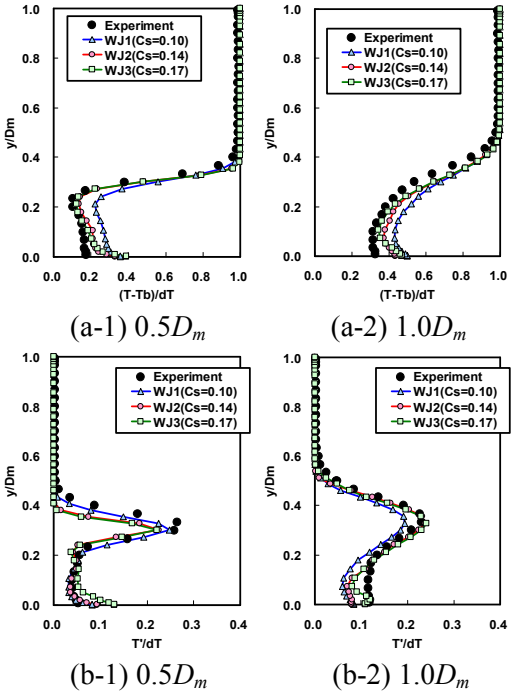

(a-1) 0.5D_m (a-2) 1.0D_m

(b-1) 0.5D_m (b-2) 1.0D_m

Fig. 13: Vertical profiles of (a) time average and (b) fluctuation intensity of temperature through the main pipe center axis at two typical positions in the wall jet case.

Figures 13 (a) and (b) respectively show vertical profiles of the time-averaged fluid temperature and the fluid temperature fluctuation intensity on the symmetric axial cross section at (1) 0.5D_m and (2) 1.0D_m downstream from the connecting point. The time-averaged temperature difference (T-T_b) as shown in Fig. 13(a) and the fluctuation intensity T' as shown in Fig. 13(b) were normalized by the fluid temperature difference before mixing dT=T_m-T_b. The fluid temperature in wake region (y/D_m<0.2) as the results of Cs=0.1 simulation was about 10% of dT(=15°C) higher than that of the experiment. In the simulation with Cs=0.1, the distinguishable hairpin vortex structures as shown in Fig. 8(b) did not appear and small-scale scattered vortices were mainly observed. When the branch pipe jet entered into the main pipe flow, shear stress was induced around the jet and the shear stress acted as driving force of the vortex generation. It could be considered that shear stress in case of Cs=0.1 was not enough to generate the hairpin vortex structure. The small-scale scattered vortices generated in the simulation with Cs=0.1. The small-scale vortices might promote the thermal mixing between the hot main pipe flow and the cold branch pipe jet. And then the fluid temperature in the wake was higher than that in the simulations with Cs=0.14 and 0.17 in which the large-scale hairpin vortices were successfully generated as shown in Fig. 13(b). Thus, the simulation with Cs=0.14 could decrease the temperature in the wake. Profiles of fluid temperature of the numerical simulation with Cs=0.14 were almost the same as those of the experiment. Typical temperature difference between the experiment and the numerical results of Cs=0.14 (WJ2) was at 2.3 °C in 15 °C (=dT) as temperature difference before mixing.

It can be recognized that the numerical results with Cs=0.14 are more appropriate ones than other results. In near wall region, the numerical results indicate that modifications are still needed in thermal diffusion because the fluid temperature near the wall region is still higher than that in experiment as shown in Fig. 13(a).

5. CONCLUSION

Numerical simulations of thermal mixing phenomena in a T-pipe were performed as a part of the V&V process of the numerical simulation code MUGTHES. A step-by-step strategy in numerical estimation method development for the thermal fatigue on the CIP in the JSFR from small-scale to large-scale examinations was introduced. V&V process for the step-by-step development steps were considered in order to prepare a potentially applicable numerical simulation code with necessary models and an estimation method for thermal fatigue estimation in the JSFR. The verification to confirm accuracy of the numerical schemes were conducted through several numerical simulations for fundamental problems at laminar flow conditions and the validation were conducted through the examinations in fundamental problems and relatively small-scale element experiments at turbulence conditions. In the

validation process, a concept of the PIRT was utilized in order to specify the problems on the subject to thermal striping phenomena in the T-pipe. A flow pattern map of the branch pipe jet in the main stream categorized by the inertia valance between that of the branch pipe jet and that of the main stream was introduced and it was explained that the map could be supported by knowledge in the jet in cross-flow investigation. Numerical simulations of thermal striping phenomena in the T-pipe at an impinging jet and a wall jet cases were conducted by using the MUGTHES with the LES approach. By the comparison of velocity and fluid temperature distributions between the numerical simulation and the experimental results in the WATLON experiment, the applicability of the MUGTHES to thermal striping phenomena in the T-pipe was confirmed. The LES approach of the MUGTHES with wall function model and the standard Smagorinsky model in Cs=0.14 was applicable in this study. The fundamental mechanisms of thermal mixing in the T-pipe at the impinging jet and the wall jet conditions were clarified thought the numerical simulations. Hairpin-shaped large-scale vortex structures were identified in front surface of the branch pipe jet at the impinging jet case and they were also behind the jet at the wall jet case. It was indicated that the large-scale vortex structure at each case had an important role in significant temperature fluctuation generation on the pipe surface.

REFERENCE

M. S. Acalar, C. R.Smith, “A Study of Hairpin Vortices in A Laminar Boundary Layer. Part 2. Hairpin Vortices generated by Fluid injection”, *J. Fluid Mech.*, 175: 43-83, (1987).

AIAA G-077-1998(2002), “Guide for the Verification and Validation of Computational Fluid Dynamics Simulations”.

ANS, “American National Standard Guidelines for the Verification and Validation of Scientific and Engineering Computer programs for the Nuclear Industry”, ANSI/ANS-10.4-1987 (R1998).

ASME, “Standard for Verification and Validation in computational Fluid Dynamics and Heat Transfer”, ASME V&V 20-2009, (2009).

A. J. Chorin, "Numerical Solution of the Navier-Stokes Equations", *Math. Comput.*, 22, 745-762 (1968).

A. Nakamura, et al., “Numerical Investigation of Thermal Striping at a Mixing Tee Using Detached Eddy Simulation”, *Proc. of NURETH-13*, N13P1074, Kanazawa, Japan, Sept. 27-Oct. 2 (2009).

M. K. Denham, M. A. Patrick, “Laminar Flow over A Downstream-facing Step in A Two-Dimensional Flow Channel”, *Trans. Inst. Chemical Engineers*, Vol.52, pp.361-367 (1974).

T. F. Fric, A. Roshiko, “Vortical structure in the wake of a transverse jet”, *J. Fluid Mech.*, 279, 1-47, (1994).

U. Ghia, et al., “High-Re Solutions for Incompressible Flow Using the Navier-Stokes Equations and Multigrid Method”, *Journal of Computational Physics*, 48, 387-411 (1982).

J. Gullbrand, F.Chow, “The effect of numerical errors and turbulence models in large-eddy simulations of channel flow with and without explicit filtering”, *J. Fluid Mech.*, 495, 323–341, (2003).

H. Hibara, et al., “Flows in T-Junction Piping System: 1st Report, Flow Characteristics and Vortex Street Formed by Branch Pipe Flow”, *Trans. of JSME*, B, 70(693), 1192-1200, (2004). [in Japanese]

M. Ichimiya, et al., “A Next Generation Sodium-Cooled Fast Reactor Concept and Its R&D Program”, *Nuclear Engineering and Technology*, 39, 171-186 (2007).

M. Igarashi, et al., “Study on Fluid Mixing Phenomena for Estimation of thermal Striping in a Mixing Tee”, *Proc. of NURETH-10*, No.A00512, Seoul, Korea, October 5-9, (2003).

JSME, “Guidline for Evaluation of High-Cycle Thermal Fatigue of a Pipe”, JSME S017-2003 (2003).

T. Kajishima, et al., “High-Order Finite Differential Method for Incompressible Flows”, *Trans. of JSME*, B 63(614), 3247-3254 (1997). [in Japanese]

H. Kamide, et al., “Study on mixing behavior in a tee piping and numerical analyses for estimation of thermal striping”, *Nucl. Eng. Des.*, 239, 58–67 (2009).

N. Kasagi, A. Matsunaga, “Three-Dimensional Particle-Tracking Velocimetry Measurement of Turbulence Statistics and Energy Budget in a Backward-Facing Step Flow”, *Int. J. Heat and Fluid Flow*, Vol. 16, No. 6, pp.474-485, (1995).

N. Kasahara, et al., “Thermal Fatigue Estimation Method Based on Power Spectrum Density Functions against Fluid Temperature Fluctuations”, *Proc. of ASME PVP2005*, PVP2005-71307, Denver, USA, July 17-21, 2005, 503-509 (2005).

N. Kimura, et al., “Study on Convective Mixing Phenomena in Parallel Triple-jet along Wall – Comparison of Temperature Fluctuation Characteristics between Sodium and Water –”, *Proc. of*

NURETH-11, Paper: 427, Avignon, France, Oct. 2-6, (2005).
N. Kimura, et al., "Development of High Cycle Thermal Fatigue Evaluation Method based on Time Interval of Peak-to Peak of Fluid Temperature", *Proc. of ASME PVP2010*, PVP2010-25595, Bellevue, Washington, USA July 18-22 (2010).
N. Kimura, et al., "Study on Convective Mixing for Thermal Striping Phenomena - Experimental Analyses on Mixing Process in Parallel Triple-Jet and Comparisons between Numerical Methods -", *Proc. of ICONE9*,No.4, Nice, France, April 8-12, (2001).
J. Kobayashi, et al., "Study on Thermal Striping at UIS of Advanced Loop Type Fast Reactor (Water Experiment using a 1/3 Scale 60 Degree Sector Model)", *Proc. of ICONE17*, ICONE17-75575, Brussels, Belgium, July 12-16, (2009).
IAEA, Validation of Fast Reactor Thermomechanical and thermohydraulics codes, TECDOC-1318, (2002).
Y. M. Marzouk and A. F. Ghoniem, "Vorticity structure and evolution in a transverse jet", *J. Fluid Mech.*, 575: 267–305 (2007).
Y. Morinishi and T. Kobayashi, "A Study on Wall Boundary Condition in LES", *Trans. of JSME*, B 55(511), 615-623 (1989). (in Japanese)
A. Nordgen, "Thermal Fluctuation in Mixing Tees (Experiences, Measurements, Prediction and Fixes)", *Proc. of SMiRT7*, D1/2, pp.7-13, Chicago, IL USA, August 22-26 (1983).
W. L. Oberkampf, T. G. Trucano, "Verification and Validation in Computational Fluid Dynamics", SANDIA REPORT SAND2002-0529, (March 2002).
K. Ohyama, O. Watanabe, H. Yamano, "Conceptual Design for Japan Sodium-Cooled Fast Reactor (2): Thermal-Hydraulic Design for Reactor Upper Sodium Plenum in JSFR", *Proc. of ICAPP '09*, Paper 9296, Tokyo, Japan, May 10-14, (2009).
S. B. Pope, Turbulent Flows, Cambridge University Press, Cambridge, UK, Sec.13.4, (2000).
S. Chapuliot, et al., "Hydro-thermal-mechanical analysis of thermal fatigue in a mixing tee", *Nucl. Eng. Des.*, 235, pp.575-596, (2005).
A. Pradera, et al., "A Numerical Study of Fluid Flow Past A Circular Cylinder at Re=3900 and A Practical Approach to Noise Prediction", *Proc. of ICSV14*, Cairns, Australia, 9-12 July, (2007).
Y. Sata, et al., "Turbulent Air Flow Measurement Using Three-Dimensional Particle Tracking Velocimetry", *Trans. of JSME*, B 60(571), 865-871 (1994). (in Japanese).
R. Sau, K. Mahesh, "Dynamics and Mixing of Vortex ring in Crossflow", *J. Fluid Mech.* 604, 384-409.(2008).
M. Tanaka, et al., "Study on Mixing Phenomena in T-pipe junction - Temperature measurement test in Pipe by Liquid Crystal Sheet -", JAEA-Research 2006-046, (2006). [in Japanese]
M. Tanaka, et al., "Thermal Mixing in T-junction Piping System concerned with High-Cycle Thermal Fatigue in Structure", *Proc. of NTHAS6*, PN6P1039, Okinawa, Japan, Nov. 24- 27, (2008).
M. Tanaka, et al., "Numerical Investigation of Thermal Striping near Core Instruments Plate around Control Rod Channels in JSFR", *Proc. of NURETH-13*, N13P1190, Kanazawa, Japan, Sept. 27-Oct. 2, (2009a).
M. Tanaka, et al., "Numerical Simulation of Thermal Striping Phenomena in a T-Junction Piping System Using Large Eddy Simulation", *J. of Power and Energy Systems*, 3(1), 237-248 (2009b).
M. Tanaka, Ph.D. thesis, University of Tsukuba, Tsukuba, Japan (2010). [in Japanese]
J. C. Tannehill, et al., Computational Fluid Mechanics and Heat Transfer (2nd Ed.), Taylor&Francis, Levittown, USA, Sec.5.7, (1997).
L. Temmerman, et al., "Investigation of Wall Function Approximations and Subgrid-Scale Models in Large Eddy Simulation of Separated Flow in a Channel with Streamwise Periodic Constrictions", *Int. J. Heat and Fluid Flow*, 24, 157-180 (2003).
G. De Vahl Davis, "Natural Convection of air in a Square Cavity: A Bench Mark Numerical Solution", *International Journal for Numerical Methods in Fluids*, Vol.3 Issue 3, pp.249-264, (1983).
G.E.Wilson, B.E.Boyack,"The role of the PIRT process in experiments, code development and code applications associated with reactor safety analysis", *Nucl. Eng. Des.*, 186, pp.23–37, (1998).
R.Martinuzzi, C.Tropea, "The Flow Around Surface-Mounted, prismatic Obstacles Placed in a Fully Developed Channel Flow", *Journal of Fluids Engineering*, Vol.115, pp.85-92 (1993).
S. Muppidi, K. Mahesh, "Direct numerical simulation of round turbulent jets in crossflow", *J. Fluid Mech.*, 574: 59-84 (2007).